Published in final edited form as:
J Magn Reson Imaging. 2012 April ; 35(4): 938–942. doi:10.1002/jmri.23531.

Unequivocal Identification of Brown Adipose Tissue in a Human Infant

Houchun H. Hu, Ph.D.[1], **Jason Tovar, M.D.**[2], **Zdena Pavlova, M.D.**[2], **Michelle L. Smith, B.A.**[1], and **Vicente Gilsanz, M.D., Ph.D.**[1]

[1]Department of Radiology, Children's Hospital of Los Angeles, Keck School of Medicine, University of Southern California, Los Angeles, California, USA

[2]Department of Pathology, Children's Hospital of Los Angeles, Keck School of Medicine, University of Southern California, Los Angeles, California, USA

Abstract

We report the unique depiction of brown adipose tissue (BAT) by MRI and computed tomography (CT) in a human three month-old infant. Based on cellular differences between BAT and more lipid-rich white adipose tissue (WAT), chemical-shift MRI and CT were both capable of generating distinct signal contrasts between the two tissues and against surrounding anatomy, utilizing fat-signal fraction metrics in the former and X-ray attenuation values in the latter. While numerous BAT imaging experiments have been performed previously in rodents, the identification of BAT in humans has only recently been described with fusion positron emission and computed tomography in adults. The imaging of BAT in children has not been widely reported and furthermore, MRI of human BAT in general has not been demonstrated. In the present work, large bilateral supraclavicular BAT depots were clearly visualized with MRI and CT. Tissue identity was subsequently confirmed by histology. BAT has important implications in regulating energy metabolism and non-shivering thermogenesis and has the potential to combat the onset of weight gain and the development of obesity. Current findings suggest that BAT is present in significant amounts in children and that MRI and CT can differentiate BAT from WAT based on intrinsic tissue properties.

Keywords

brown adipose tissue; white adipose tissue; histology; human; fat-signal fraction; X-ray attenuation

INTRODUCTION

Recent findings of metabolically active brown adipose tissue (BAT) in adult humans by fusion positron emission and computed tomography (PET/CT) have reinvigorated research towards the tissue's role in energy metabolism and its potential to counteract weight gain and development of obesity (1–3). In contrast to white adipose tissue (WAT), which functions to store fat, BAT is responsible for non-shivering thermogenesis that is facilitated by a special uncoupling protein (UCP-1). BAT is also highly vascularized, rich in mitochondria, innervated by the sympathetic nervous system, and can be metabolically active. WAT is characterized by adipocytes that contain a single large intracellular lipid

Corresponding Author Houchun Harry Hu, Ph.D., Children's Hospital of Los Angeles, Department of Radiology, 4650 Sunset Boulevard, MS #81, Los Angeles, California (CA), USA. 90027, Telephone: (323)-361-2688, Fax: (323)-361-1510, hhu@chla.usc.edu, houchunh@usc.edu.

droplet, a peripherally located nucleus, limited cytoplasm, and very little intracellular and extracellular water. In comparison, BAT adipocytes are generally smaller in size, contain multiple intracellular lipid droplets, a centrally-located nucleus, greater cytoplasm volume replete with mitochondria organelles, and more intracellular and extracellular water (4–7).

While PET/CT has provided the ability to visualize BAT, the technique has key limitations. First, it is restricted to oncology patients and is not applicable to the general population, particularly children, due to significant radiation exposures and ethical restrictions. Second, PET/CT can only detect metabolically active BAT that uptakes the injected radionuclide tracer. Metabolically inactive BAT is not observed. Past literature has shown that the prevalence of BAT in children is significantly greater than in adults (8–10). Therefore, the development of alternative techniques to identify and quantify BAT in pediatric populations is critically needed to advance our knowledge of the tissue's physiological role.

MRI represents the most promising modality to address the limitations of PET/CT. It involves no ionizing radiation and requires no radionuclides. It can be safely implemented with minimal risk in healthy children and adults. Over the past few years, several works have investigated the feasibility of detecting BAT in rodents by exploiting the intrinsic cellular differences between BAT and WAT to generate signal contrasts based on fat-signal fraction from chemical-shift MRI (11), T1 relaxation (12), and intermolecular zero-quantum coherence spectroscopy (13).

In this work, we report the unequivocal identification of metabolically inactive BAT in a three month-old human infant body by MRI and independently by computed tomography (CT). Furthermore, the tissue's identity was confirmed by post-mortem histology. While T1 and T2-weighted MRI and CT examination of BAT in a newborn have been reported in a previous case study (14), the present work provides additional corroboration of the tissue's identity by histology. Utilizing fat-water chemical-shift MRI and CT, we demonstrate in this patient that the difference in cellular water and fat content between BAT and WAT lends to unique complementary signal contrasts between the two tissues, based on fat-signal fraction in the former (11), and X-ray tissue attenuation (e.g. Hounsfield Units - HUs) in the latter (15). Namely, BAT has a lower fat-signal fraction than WAT as observed on chemical-shift MRI, and BAT has more positive X-ray attenuation HUs than WAT as observed on CT. The basis of these signal contrasts has been previously explained in detail in the cited references.

MATERIALS and METHODS

The protocol for this study was approved by the Institutional Review Board of the ___ (removed for blinded review), where the imaging and post-mortem examinations were performed. This 95 day-old, full term female infant developed severe respiratory distress a few hours after birth. Due to the severity of the respiratory distress and persistent pulmonary hypertension, the patient was placed on extracorporeal membrane oxygenation at one month of age. The diagnosis of alveolar capillary dysplasia was suspected when the patient did not respond to treatment and progressive dilatation of the right ventricle was depicted by echo-cardiography. A FOXF1 heterozygous genetic mutation was detected and supported the primary diagnosis of alveolar capillary dysplasia, which was confirmed at autopsy.

Within 48 hours after the patient was pronounced deceased, MRI, CT, and tissue biopsy procedures were performed. First, MRI was implemented on a 3 Tesla whole-body human platform (Achieva, R2.6.3, Philips Healthcare, Cleveland, Ohio). The infant's head, neck, chest, and thorax regions were placed inside an eight-channel head coil. The body was not frozen and was imaged at a room (MRI suite) temperature of approximately 22 degrees Celsius. A chemical-shift two-point 3D spoiled gradient echo pulse sequence from the

vendor was utilized (16). Imaging parameters for the coronal acquisition were: TR = 3.9 msec, TE1/TE2 = 1.4/2.5 msec, full echoes, Cartesian acquisition, flip angle = 5°, FOV = 35 cm (superior/inferior) and 17.5 cm (right/left), 350×350 acquisition matrix, 2 mm overlapping slices (reconstructed to 1 mm), number of averages = 2, no parallel imaging acceleration, and bandwidth = 1.3 kHz/pixel. For 100 slices (10 cm effective coverage), the acquisition time was 68 seconds, and the reconstructed spatial resolution was 1 mm isotropic. Fat-only, water-only, and fat-signal fraction maps (fat/(fat + water)) were generated for the acquired 3D volume (17).

A subsequent CT exam was performed on a whole-body human platform (LightSpeed QX, R10.5, General Electric Healthcare, Waukesha, Wisconsin). Acquisition mode was helical and imaging parameters were: kVp = 120 Volts, 160 axial slices of 2.5 mm thickness, and an in-plane resolution of 0.54 mm. The acquisition time was approximately one minute.

Supraclavicular BAT depots visually identified on MRI and CT images were presented to two pathologists. After reviewing the images together with the radiologist involved in this work, the pathologists were instructed to extracted two tissue samples from the sites of interest, one from the left and one from the right supraclavicular BAT depots. The biopsies were taken from the anterior deep soft tissue pad bound by the trapezius muscle posteriorly, the sternocleidomastoid muscle medially, and the clavicle inferiorly. The radiologist was present at the time of biopsy to verify tissue location. Extracted samples were fixed in formalin, embedded in paraffin, and stained with hemotoxylin and eosin for visual analysis under miscroscope.

Image post-processing was performed with SliceOmatic segmentation software (Tomovision, Inc., Quebec, Canada). Fat-signal fraction and HU measures were computed after segmenting across all coronal (MRI) and axial (CT) slices that encompassed the bilateral supraclavicular BAT depots. The total volume of supraclavicular BAT was also measured.

RESULTS

From MRI data, a total volume of 17.4 ml of supraclavicular BAT was determined. Analysis of the CT data yielded 16.9 ml. Figure 1A illustrates native coronal (top row) and reformatted axial (bottom row) images of the neck and chest from chemical-shift MRI. Complementary fat-only and water-only images are shown in the first and secondly columns, respectively, along with the corresponding colorized fat-signal fraction map in the third column. Arrowheads in the fat-only image point to the layer of lipid-rich subcutaneous WAT, which exhibits strong signal intensity. On the corresponding water-only image, WAT is expectedly dark and devoid of signal. In the fat-signal fraction map, red coloring (> 90%) of the WAT region confirms that the tissue is predominantly composed of lipids. In contrast, arrows in the fat-only image point to evident bilateral BAT depots, adjacent to the scapula and clavical. Note that the BAT depots exhibit intermediate gray signal intensities and are visible on both the fat and water images. It is hypointense to that of WAT in the fat-only image and oppositely hyperintense to that of WAT in the water-only image. Blue, green, and yellow representations of these regions in the fat-signal fraction map suggest a lower fat to water ratio than WAT. Based on segmentations of the MRI data, the average fat-signal fraction across the entire bilateral supraclavicular BAT depots was 41.9 ± 6.25%.

Figure 1B illustrates anatomically matching CT images shown on a colormap of Hounsfield Units, a measure of X-ray attenuation and a reflection of a tissue's apparent density. Note that the subcutaneous WAT layer is represented in purple, in the range of −60 to −100 HUs. In contrast, the bilateral BAT depots are distinctly visible in shades of green and blue,

suggestive of greater water content and tissue density and more positive HUs. Note that BAT HUs values remain negative, indicative of fat content. Based on segmentations of the CT data, the average value across the entire bilateral supraclavicular BAT depots was −20.76 ± 3.37 HUs. On both MRI fat-signal fraction and CT HU data, note that the identified metabolically inactive BAT from this infant case occupies a signal range that is intermediate to WAT and surrounding musculature and that tissue signal contrast is visually recognizable.

Figure 1C and D illustrate corroborating histological specimens taken from the bilateral supraclavicular BAT depots. In the first sample, black arrowheads on the right side of the image point to large uni-locular WAT adipocytes. In contrast, blue arrowheads point to multi-locular BAT adipocytes that are highly perfused by capillaries (blue arrows). Note that multiple lipid vacuoles can be clearly identified within each BAT adipocyte, while only a single lipid vacuole can be observed in each of the WAT cells. Figure 1D shows a histology slide at two-fold greater magnification of the second sample, where the multi-locular characteristic of BAT is evident.

DISCUSSION

Utilizing independently chemical-shift MRI, CT, and histology, and presented with a unique opportunity, we have demonstrated the feasibility of imaging to identify metabolically inactive BAT based on intrinsic tissue properties in a three-months-old human infant. The difference in appearance between BAT and WAT on both images and histology was marked. Currently PET/CT remains the gold-standard technique to examine metabolically active brown adipose tissue and it has been utilized in many studies involving adult patients. In contrast, the number of BAT studies in pediatric patients has been few, due to the elevated risk of ionizing radiation and radionuclide tracer usage by PET/CT. Furthermore, PET/CT exams are not permitted in healthy children. However, BAT has a significantly higher prevalence in children. Young cohorts thus represent an ideal population to further examine the potential relationships of BAT to muscle development, puberty, disease state, and the accumulation of white adipose tissue. Thus, MRI represents the most appropriate modality to overcome the limitations of PET/CT. The development of rapid, repeatable MRI techniques to characterize BAT is critically needed to advance our knowledge of this tissue's physiology.

In this patient, we specifically reviewed the neck region on both MRI and CT data for indications of BAT as the supraclavicular depot has been reported in literature to be to the largest and most prominent and recognizable BAT site in both rodents and humans. While multiple other BAT sites exist within the underarm and mediastinum and around the spine and kidneys (18), we did not observe any evident MRI or CT imaging signatures suggestive of BAT in these areas in this infant. BAT often exists in small clusters of 50–100 cells surrounded by large numbers of white adipocytes and have also been shown to contain lipid vacuoles of varying sizes (6). Despite the high spatial resolution employed in this work, accurate detection of very small BAT depots (e.g. a few groups of isolated cells) without confounding errors from volume averaging remains challenging. The lack of observation on the imaging data of BAT at locations other than the prominent supraclavicular region does not necessarily imply that the tissue was non-existent in this infant at those locations. It however does raise the possibility that current imaging techniques alone are not yet sensitive enough to detect isolated colonies of BAT.

One limitation of this work was that for chemical-shift MRI, we did not employ the most accurate sequence and approach to compute fat-signal fraction. A plethora of recent works has shown that in order to estimate accurately the underlying tissue proton-density fat

fraction, one must account for numerous confounding factors such as T1 bias, T2* relaxation, noise bias, and the multiple spectral peaks of fat (19–21). On our current clinical MRI system, the two-point 3D spoiled gradient echo technique was the only available chemical-shift pulse sequence available from the manufacturer. While we attempted to minimize T1 bias by employing a small flip angle (19), the manufacturer software employed only a single peak fat model in image reconstruction and did not account for additional T2* relaxation. Thus while we recognize that the fat-signal fraction map shown in results does not reflect accurately the true underlying tissue proton-density fat fraction of BAT and WAT, we anticipate that the above confounding factors to have only a marginal and systematic effect on the fat-signal fraction. We nonetheless expect distinct differences in fat-signal fraction between BAT and WAT to exist, with BAT values less than that of WAT, had confounding factors been addressed (11).

We further recognize that chemical-shift MRI may lack the sensitivity and specificity as an independent method to adequately identify BAT *in vivo*, especially in cases where the tissue has a very low fat content (fat-signal fraction) or where *a priori* knowledge of tissue depot locations in the anatomy is not known or assumed. Prior literature has reported that BAT can have highly varying levels of intracellular fat content, reflecting the relative functional state of the tissue (22, 23). When the tissue is metabolically inactive, fat content can be quite high and the tissue can exhibit a WAT-like appearance in both imaging and histology (24). Conversely, the tissue can also exhibit nearly no fat content, representative of a metabolically depleted state. At these two extremes, we anticipate that chemical-shift MRI will have very low sensitivity in the identification of BAT and may thus not be the most suitable pulse sequence choice. To further complicate the matter, recent findings have also suggested that certain BAT cells can differentiate from WAT progenitors and exhibit an intermediate phenotype that satisfies both classical definitions of BAT and WAT (25, 26). Thus, the detection limit of BAT by chemical-shift MRI remains to be investigated and the technique may likely serve as only one in a compilation of complementary pulse sequences that collectively will unambiguously identify and characterize BAT *in vivo*. Additionally, given that BAT imaging very likely requires sub-millimeter spatial resolution, the issue of adequate signal-to-noise ratio (SNR) from chemical-shift MRI or any other pulse sequence that yields BAT vs. WAT tissue contrast remains to be explored with appropriate protocols and coil arrays.

In the present work, we employed a MRI protocol with two signal averages and no parallel imaging to achieve a scan time of approximately one minute. Keeping spatial resolution and the number of slices constant, we have been testing a protocol for imaging live healthy adults with no signal averaging and two-fold parallel imaging. Utilizing a 16-channel neurovascular coil array in lieu of the 8-channel head coil used in the current study for improved SNR, the resulting scan time was reduced to less than 20 seconds, within the breath-hold regime. However, in the region of suspected supraclavicular BAT depots, respiratory motion has not a major hindrance. In addition, we are further investigating a dedicated coil array and imaging setup for studies in live neonates and infants, in particular at 1.5 Tesla.

Lastly, it must be recognized that the current imaging results were obtained from a post-mortem body, and more critically in a patient with known disease. Our measured MRI fat-signal fractions of BAT can potentially be further confounded by unrelated tissue edema, lack of blood flow, a lowered body temperature, which causes deviations in the presumed fat-water chemical shift, and possible variations in local tissue T1 and T2 values, in comparison to a live healthy subject imaging scenario. The presence of edema and the lack of blood flow can similarly affect the apparent HU measures of BAT in CT. However, irrespective of these confounding factors which are likely to introduce only a marginal yet

systematic nominal bias in the fat-signal fraction and HU estimates of BAT and WAT, we expect there to exist in a majority of cases a fundamental difference in signal contrast (fat-signal fraction, tissue density) between functionally active BAT where fat is being metabolized and inert WAT, both *in situ* and *in vivo*.

In conclusion, the intrinsic cellular differences between BAT and WAT adipocytes give rise to distinctive and complementary signal contrasts between the two tissues in chemical-shift MRI and independently in CT. Observations from this pediatric case study are consistent with previous literature findings in mice (11) and human adolescents (15). This work supports non-ionizing MRI as a suitable imaging modality to further study BAT on a large scale in healthy populations, especially in children where BAT is more prevalent. Furthermore, MRI represents a promising alternative to current gold-standard PET/CT. Many additional distinctive features of BAT are known but have not yet been explored in-depth by MRI and MR spectroscopy. For example, BAT's immense vasculature lends itself potentially to well-established MRI perfusion techniques such as arterial-spin-labeling that can quantify local blood flow. Techniques that are sensitive to $T2^*$ relaxation as a consequence of fluctuating levels of oxy- and deoxy- hemoglobin in blood are being considered. Signal contrasts between BAT and WAT, such as diffusion, local tissue temperature (27), and targeted molecular imaging of the mitochondria, have not been investigated and can possibly be combined with chemical-shift imaging. Lastly, recent advances in fusion PET/MR also holds promise as an adjunct tool for combined morphological and functional BAT imaging. Given that BAT appears to be a highly dynamic and elusive tissue that can exist in a variety of states and exhibit a wide spectrum of characteristics, it is becoming increasingly apparent with recent literature findings that more than one MRI pulse sequence or imaging approach is likely needed to positively identify the tissue *in vivo*.

Acknowledgments

Funding Support

National Institutes of Health

Gilsanz – R21DK090778, Hu – K25DK087931

References

1. van Marken Lichtenbelt WD, Vanhommerig JW, Smulders NM, et al. Cold-activated brown adipose tissue in healthy men. N Engl J Med. 2009; 360:1500–1508. [PubMed: 19357405]
2. Cypess AM, Lehman S, Williams G, et al. Identification and importance of brown adipose tissue in adult humans. N Engl J Med. 2009; 360:1509–1517. [PubMed: 19357406]
3. Virtanen KA, Lidell ME, Orava J, et al. Functional brown adipose tissue in healthy adults. N Engl J Med. 2009; 360:1518–1525. [PubMed: 19357407]
4. Enerback S. Human brown adipose tissue. Cell Metab. 2010; 11:248–252. [PubMed: 20374955]
5. Cannon B, Nedergaard J. Brown adipose tissue: function and physiological significance. Physiol Rev. 2004; 84:277–359. [PubMed: 14715917]
6. Cinti S. The role of brown adipose tissue in human obesity. Nutr Metab Cardiovasc Dis. 2006; 16:569–574. [PubMed: 17113764]
7. Nedergaard J, Cannon B. The changed metabolic world with human brown adipose tissue: therapeutic visions. Cell Metab. 2010; 11:268–272. [PubMed: 20374959]
8. Gelfand MJ, O'Hara SM, Curtwright LA, Maclean JR. Pre-medication to block 18F-FDG uptake in the brown adipose tissue of pediatric and adolescent patients. Pediatr Radiol. 2005; 35:984–990. [PubMed: 15988582]

9. Gilsanz V, Chung SA, Jackson H, Dorey FJ, Hu HH. Functional brown adipose tissue is related to muscle volume in children and adolescents. J Pediatr. 2011; 158:722–726. [PubMed: 21168855]
10. Drubach LA, Palmer EL, Connolly LP, Baker A, Zurakowski D, Cypess AM. Pediatric brown adipose tissue: detection, epidemiology, and differences from adults. J Pediatr. 201110.1016/j.jpeds.2011.06.028
11. Hu HH, Smith DL Jr, Nayak KS, Goran MI, Nagy TR. Identification of brown adipose tissue in mice with fat-water IDEAL-MRI. J Magn Reson Imaging. 2010; 31:1195–1202. [PubMed: 20432356]
12. Hamilton G, Bydder M, Smith DL Jr, Nayak KS, Hu HH. Properties of brown and white adipose tissue measured by 1H MRS. J Magn Reson Imaging. 2011; 34:468–473. [PubMed: 21780237]
13. Branca RT, Warren WS. In vivo brown adipose tissue detection and characterization using water-lipid intermolecular zero-quantum coherences. Magn Reson Med. 2011; 65:313–319. [PubMed: 20939093]
14. Carter BW, Schucany WG. Brown adipose tissue in a newborn. Proc (Bayl Univ Med Cent). 2008; 21:328–330. [PubMed: 18628932]
15. Hu HH, Chung SA, Nayak KS, Jackson HA, Gilsanz V. Differential computed tomographic attenuation of metabolically active and inactive adipose tissues: preliminary findings. J Comput Assist Tomogr. 2011; 35:65–71. [PubMed: 21245691]
16. Eggers H, Brendel B, Duijndam A, Herigault G. Dual-echo Dixon imaging with flexible choice of echo times. Magn Reson Med. 2011; 65:96–107. [PubMed: 20860006]
17. Cassidy FH, Yokoo T, Aganovic L, et al. Fatty liver disease: MR imaging techniques for the detection and quantification of liver steatosis. Radiographics. 2009; 29:231–260. [PubMed: 19168847]
18. Merklin RJ. Growth and distribution of human fetal brown fat. Anat Rec. 1974; 178:637–645. [PubMed: 4856126]
19. Liu CY, McKenzie CA, Yu H, Brittain JH, Reeder SB. Fat quantification with IDEAL gradient echo imaging: correction of bias from T1 and noise. Magn Reson Med. 2007; 58:354–364. [PubMed: 17654578]
20. Yu H, Shimakawa A, McKenzie CA, Brodsky E, Brittain JH, Reeder SB. Multiecho water-fat separation and simultaneous R2* estimation with multifrequency fat spectrum modeling. Magn Reson Med. 2008; 60:1122–1134. [PubMed: 18956464]
21. Bydder M, Yokoo T, Hamilton G, et al. Relaxation effects in the quantification of fat using gradient echo imaging. Magn Reson Imaging. 2008; 26:347–359. [PubMed: 18093781]
22. Heaton JM. The distribution of brown adipose tissue in the human. J Anat. 1972; 112:35–39. [PubMed: 5086212]
23. Tanuma Y, Tamamoto M, Ito T, Yokochi C. The occurrence of brown adipose tissue in perirenal fat in Japanese. Arch Histol Jpn. 1975; 38:43–70. [PubMed: 1200786]
24. Baba S, Jacene HA, Engles JM, Honda H, Wahl RL. CT Hounsefield units of brown adipose tissue increase with activation: preclinical and clinical studies. J Nucl Med. 2010; 51:246–250. [PubMed: 20124047]
25. Barbatelli G, Murano I, Madsen L, et al. The emergence of cold-induced brown adipocytes in mouse white fat depots is determined predominantly by white to brown adipocyte transdifferentiation. Am J Physiol Endocrinol Metab. 2000; 298:E1244–1253. [PubMed: 20354155]
26. Petrovic N, Shabalina IG, Timmons JA, Cannon B, Nedergaard J. Thermogenically competent nonadrenergic recruitment in brown preadipocytes by a PPARgamma agonist. Am J Physiol Endocrinol Metab. 2008; 295:E287–296. [PubMed: 18492776]
27. Soher BJ, Wyatt C, Reeder SB, MacFall J. Noninvasive temperature mapping with MRI using chemical shift water-fat separation. Magn Reson Med. 2010; 63:1238–1246. [PubMed: 20432295]

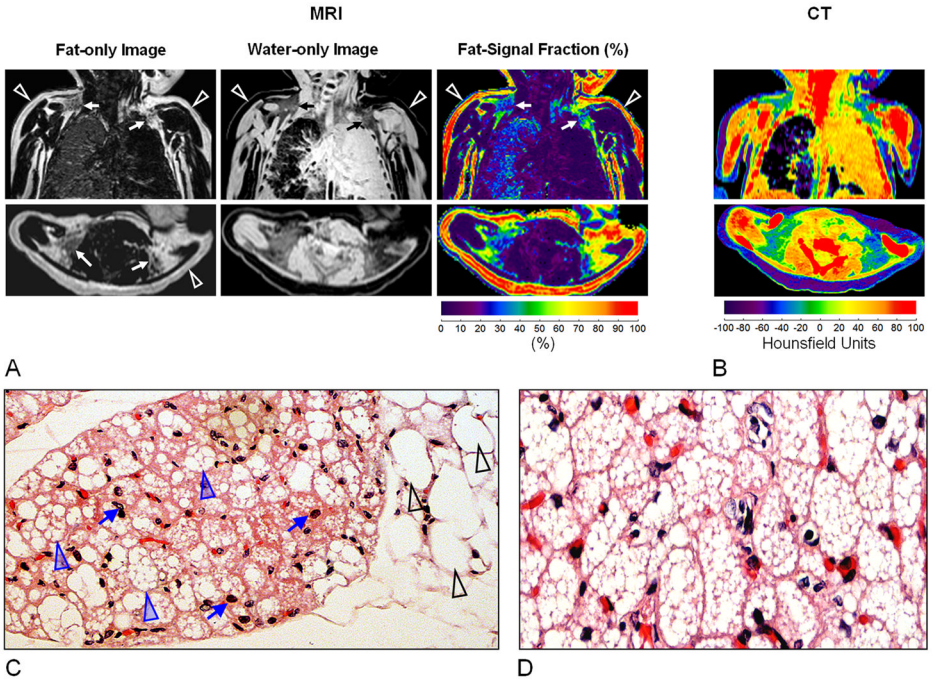

Figure 1.

(A) Brown adipose tissue (BAT) depiction by MRI, illustrating bilateral BAT depots (arrows) near the neck. Note that BAT has appreciable signal in both fat-only and water-only images. In contrast, lipid-rich subcutaneous white adipose tissue (WAT: open arrowheads) exhibits dominant signal only in the fat image. Fat-signal fraction maps show intermediate values for BAT, in contrast to WAT. Note the fluid-filled left lung. (B) On CT, WAT exhibits negative X-ray attenuation Hounsfield Units (HUs). By comparison, BAT is characterized by more positive HUs. (C) Histological specimen stained with hematoxylin and eosin at 10x magnification taken from the BAT depots. Black arrowheads point to the large white adipocytes each with a single intracellular vacuole of lipids, round in shape, and approximately 100–120 μm in size. Blue arrowheads point to smaller brown adipocytes, with multiple intracellular lipid droplets, polygonal in shape, and 25–40 μm in size. Furthermore, BAT is perfused by capillaries (blue arrows). (D) 20x magnification of another extracted tissue sample.